Hybrid-Mode Analysis of Arbitrarily Shaped Planar Microwave Structures by the Method of Lines

STEPHAN B. WORM AND REINHOLD PREGLA, SENIOR MEMBER, IEEE

Abstract — **This paper presents a method for analyzing arbitrarily shaped planar microwave structures, which is based on the method of lines and applies to both resonant and periodic structures in microstrip, slotline, and finline circuits. Numerical results are presented for some selected structures.**

I. INTRODUCTION

THE CHARACTERIZATION of planar structures (e.g., microstrip, slotline, and finline) is important in microwave integrated circuit design. The considered structures consist of two or more homogeneous layers, i.e., dielectric substrates or air regions, with various types of metallization located on the interfaces between the layers. Some typical cross sections are shown in Fig. 1

In the following, it will be assumed that the metallization has vanishing thickness and that the structures are shielded with perfectly conducting walls. Also, in cases of symmetry, magnetic walls may occur.

Recently, an efficient method for calculating the dispersion characteristics of these types of planar transmission lines was published [1], [2], which is based on the method of lines. With this method, the cross sections are discretized in one direction, whereas the other directions are treated analytically. The object of this paper is to show how the method of lines may be extended to two-dimensional discretization for the analysis of resonant and periodic planar microwave structures.

In principle, arbitrarily shaped resonators may be analyzed, as is demonstrated for a triangular microstrip resonator. The method is accurate enough to derive the characteristic properties of discontinuities from the calculated resonant frequencies. As an example, the end effect of a shorted slotline is investigated.

Another important class of planar microwave structures is formed by periodic structures (e.g., meander-type delay lines). Periodic structures have also been proposed for the phase-equalization of odd and even modes in order to improve the properties of microstrip couplers [3]. Here, the method of lines may also be applied successfully.

Manuscript received June 21, 1983; revised September 26, 1983. This work was supported in part by the Deutsche Forschungs gemeinschaft.

The authors are with the Department of Electrical Engineering, Fernuniversität, P.O. Box 940, D-5800 Hagen, Federal Republic of Germany.

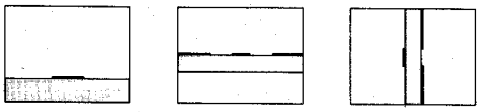

Fig. 1. Cross sections of some planar microwave structures.

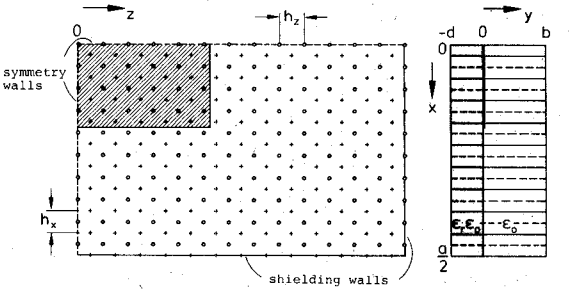

Fig. 2. Position of the discretization lines for a rectangular microstrip resonator (+ for Ψ^e and ∘ for Ψ^h lines).

Advantages of the presented method are its easy formulation and its simple convergence behavior. There is no need to specify specially suited expansion functions, which is particularly advantageous to the analysis of odd-shaped resonators or if the expansion functions would be complex quantities, as is the case with periodic structures. With conventional finite difference methods, large systems of equations are solved directly. With this method a problem-oriented discrete Fourier transform is applied, so the main part of the problem is solved in a transformed domain, where only diagonal matrices occur. The final equations in the original domain are solved with matrices of considerably reduced size.

II. THE ANALYSIS OF PLANAR RESONATORS

The principles of the method of analysis will be demonstrated for a simple rectangular microstrip resonator (Fig. 2). The extension to multilayered structures like slotlines and suspended striplines is straightforward.

The electromagnetic field in each homogeneous region is described by two scalar potential functions Ψ^e and Ψ^h that satisfy the Helmholtz equation and the boundary conditions at the shielding and symmetry walls.

The field components are then found from

$$\vec{E} = \nabla \times \nabla \times (\Psi^e \vec{u}_z)/j\omega\epsilon - \nabla \times (\Psi^h \vec{u}_z)$$
$$\vec{H} = \nabla \times (\Psi^e \vec{u}_z) + \nabla \times \nabla \times (\Psi^h \vec{u}_z)/j\omega\mu_0 \quad (1)$$

0018-9480/84/0200-0191$01.00 ©1984 IEEE

where the time-dependence according to $\exp(j\omega t)$ is assumed. At the air–dielectric interface, the continuity conditions for the tangential electric and magnetic field components have to be satisfied as follows:

$$
\begin{aligned}
E_{x\mathrm{I}} - E_{x\mathrm{II}} &= \frac{1}{j\omega\epsilon_r\epsilon_0}\frac{\partial^2\Psi_{\mathrm{I}}^e}{\partial x\partial z} - \frac{\partial\Psi_{\mathrm{I}}^h}{\partial y} - \frac{1}{j\omega\epsilon_0}\frac{\partial^2\Psi_{\mathrm{II}}^e}{\partial x\partial z} + \frac{\partial\Psi_{\mathrm{II}}^h}{\partial y} = 0\\
E_{z\mathrm{I}} - E_{z\mathrm{II}} &= \frac{1}{j\omega\epsilon_r\epsilon_0}\left(\frac{\partial^2\Psi_{\mathrm{I}}^e}{\partial z^2} + \epsilon_r k_0^2\Psi_{\mathrm{I}}^e\right) - \frac{1}{j\omega\epsilon_0}\left(\frac{\partial^2\Psi_{\mathrm{II}}^e}{\partial z^2} + k_0^2\Psi_{\mathrm{II}}^e\right) = 0\\
H_{x\mathrm{I}} - H_{x\mathrm{II}} &= \frac{\partial\Psi_{\mathrm{I}}^e}{\partial_y} + \frac{1}{j\omega\mu_0}\frac{\partial^2\Psi_{\mathrm{I}}^h}{\partial x\partial z} - \frac{\partial\Psi_{\mathrm{II}}^e}{\partial y} - \frac{1}{j\omega\mu_0}\frac{\partial^2\Psi_{\mathrm{II}}^h}{\partial x\partial z} = -J_z\\
H_{z\mathrm{I}} - H_{z\mathrm{II}} &= \frac{1}{j\omega\mu_0}\left(\frac{\partial^2\Psi_{\mathrm{I}}^h}{\partial z^2} + \epsilon_r k_0^2\Psi_{\mathrm{I}}^h - \frac{\partial^2\Psi_{\mathrm{II}}^h}{\partial z^2} - k_0^2\Psi_{\mathrm{II}}^h\right) = J_x
\end{aligned}
\tag{2}
$$

with

$$k_0 = \omega\sqrt{\epsilon_0\mu_0}\,.$$

The final boundary condition states, that the current density distributions J_z and J_x be nonzero or that the tangential electric field components E_z and E_x be zero on the metallized parts of the interface.

In order to solve this hybrid field problem numerically, the considered region is discretized in the x- and z-direction with meshwidths h_x and h_z, respectively. The discretization lines for Ψ^h are shifted by $h_x/2$ and $h_z/2$ with respect to the lines for Ψ^e. In this way, the lateral boundary conditions at the shielding and symmetry walls can be fitted easily and discretization error is reduced considerably, as was also found for the case of one-dimensional discretization [1], [2].

For the example of Fig. 2, the potential function Ψ^e at $x=(i-0.5)h_x$ and $z=(k-0.5)h_z$ $(i=1,\cdots,N_x;\ k=1,\cdots,N_z)$ will be denoted by Ψ_{ik}^e and interpreted as an element of the matrix $[\Psi^e]$, in which the elements are arranged in the same pattern as in the discretized structure. It should be noted, however, that $[\Psi^e]$ really has a vector character, which will become important later on.

For the first derivative of Ψ^e with respect to the x-direction, one obtains

$$\left.\frac{\partial\Psi^e}{\partial x}\right|_{\substack{x=ih_x\\ z=(k-0.5)h_z}} = \frac{\Psi_{i+1,k}^e - \Psi_{i,k}^e}{h_x} + 0\left(h_x^2\right) \tag{3}$$

or, in matrix notation

$$
h_x\frac{\partial\Psi^e}{\partial x} \rightarrow \begin{bmatrix} -1 & 1 & & \\ & \ddots & \ddots & \\ & & -1 & 1 \end{bmatrix}\begin{bmatrix} \Psi_{1,1}^e & \cdots & \Psi_{1,N_z}^e \\ \vdots & & \vdots \\ \Psi_{N_x,1}^e & \cdots & \Psi_{N_x,N_z}^e \end{bmatrix} = [D_x][\Psi^e]. \tag{4}
$$

The difference matrix $[D_x]$ depends on the lateral boundary conditions for Ψ^e (see Table I). It is the same operator matrix as used in the case of one-dimensional discretization. Here, it forms the difference between two successive rows of the matrix $[\Psi^e]$.

Because Ψ^e and Ψ^h have dual boundary conditions, the finite difference expression for the first derivative of Ψ^h becomes

$$h_x\frac{\partial\Psi^h}{\partial x} \rightarrow -[D_x]^t[\Psi^h]. \tag{5}$$

Combining (4) and (5), one obtains for the second-order derivatives

$$h_x^2\frac{\partial^2\Psi^e}{\partial x^2} \rightarrow -[D_x]^t[D_x][\Psi^e] = [D_{xx}^e][\Psi^e] \tag{6}$$

$$h_x^2\frac{\partial^2\Psi^h}{\partial x^2} \rightarrow -[D_x][D_x]^t[\Psi^h] = [D_{xx}^h][\Psi^h]. \tag{7}$$

Analogously, the difference operator for the first derivative of Ψ^e with respect to the z-direction should form the difference between two successive columns of the matrix $[\Psi^e]$. Thus, the difference matrix $[D_z]$, as taken from Table I, will operate on the transpose of the matrix $[\Psi^e]$

$$h_z\frac{\partial\Psi^e}{\partial z} \rightarrow [D_z][\Psi^e]^t \tag{8}$$

or rather

$$\rightarrow [\Psi^e][D_z]^t. \tag{9}$$

In a similar way, the finite difference expression for the second-order derivative of Ψ^e with respect to z is written as

$$h_z^2\frac{\partial^2\Psi^e}{\partial z^2} \rightarrow -[\Psi^e][D_z]^t[D_z] = [\Psi^e][D_{zz}^e]^t. \tag{10}$$

This notation provides simple compatibility with the difference operators for the x-direction, e.g.,

$$h_x h_z\frac{\partial^2\Psi^e}{\partial x\partial z} \rightarrow [D_x][\Psi^e][D_z]^t. \tag{11}$$

Working out this expression for the above example yields

$$\left.h_x h_z\frac{\partial^2\Psi^e}{\partial x\partial z}\right|_{\substack{x=ih_x\\ z=kh_z}} \simeq \Psi_{i,k}^e - \Psi_{i,k+1}^e + \Psi_{i+1,k+1}^e - \Psi_{i+1,k}^e. \tag{12}$$

It is evaluated at the discretization line for Ψ_{ik}^h from the function values at the four adjacent Ψ^e lines, so it fits well into the continuity equations (2) using only small discretization distances.

Because of the tri-diagonal structure of the difference matrices $[D_{xx}^e]$ and $[D_{zz}^e]$, the discretized Helmholtz equa-

tion

$$\frac{d^2[\Psi^e]}{dy^2} + \frac{[D_{xx}^e][\Psi^e]}{h_x^2} + \frac{[\Psi^e][D_{zz}^e]^t}{h_z^2} + \epsilon_r k_0^2[\Psi^e] = 0 \tag{13}$$

represents a system of $N_x N_z$ differential equations, that are all coupled with each other.

By means of the orthogonal transformation matrices $[T_x^e]$ and $[T_z^e]$ (see Appendix) the difference matrices are transformed into diagonal matrices

$$[T_x^e]^t[D_{xx}^e][T_x^e] = \text{diag}[d_{xx}^e] \tag{14}$$

$$[T_z^e]^t[D_{zz}^e][T_z^e] = \text{diag}[d_{zz}^e]. \tag{15}$$

So, for the elements of the transformed potential matrix

$$[U] = [T_x^e]^t[\Psi^e][T_z^e] \tag{16}$$

one obtains the uncoupled differential equations

$$\frac{d^2[U]_{ik}}{dy^2} - \kappa_{ik}^2[U]_{ik} = 0 \tag{17}$$

with

$$\kappa_{ik}^2 = -\left(\frac{[d_{xx}^e]_{ii}}{h_x^2} + \frac{[d_{zz}^e]_{kk}}{h_z^2} + \epsilon_r k_0^2\right). \tag{18}$$

The general solution to (17) may be written as a relation between $[U]_{ik}$ and its normal derivative in the planes $y = y_1$ and $y = y_2$

$$\begin{pmatrix} U(y_1) \\ \left.\dfrac{d[U]}{dy}\right|_{y_1} \end{pmatrix}_{ik} = \begin{pmatrix} \cosh\kappa_{ik}(y_1 - y_2) & \dfrac{\sinh\kappa_{ik}(y_1 - y_2)}{\kappa_{ik}} \\ \kappa_{ik}\sinh\kappa_{ik}(y_1 - y_2) & \cosh\kappa_{ik}(y_1 - y_2) \end{pmatrix}_{ik} \begin{pmatrix} U(y_2) \\ \left.\dfrac{d[U]}{dy}\right|_{y_2} \end{pmatrix}_{ik}. \tag{19}$$

By means of this relation, the boundary conditions at the top and bottom shielding can be transformed into the interface plane $y = 0$, e.g., for the substrate region one obtains with $[U(y = -d)]_{ik} = 0$

$$\left.\frac{d[U]_{ik}}{dy}\right|_{y=0} = \frac{\kappa_{ik}}{\tanh\kappa_{ik}d}[U(y=0)]_{ik}. \tag{20}$$

The other potential function Ψ^h is transformed by means of the orthogonal matrices $[T_x^h]$ and $[T_z^h]$ (see Appendix) in a similar way, so that the continuity equations (2) may be solved entirely in the transformed domain. This yields an equation of the following form:

$$\begin{pmatrix} \tilde{E}_z \\ \tilde{E}_x \end{pmatrix} = \begin{bmatrix} [\tilde{Z}_{11}] & [\tilde{Z}_{12}] \\ [\tilde{Z}_{21}] & [\tilde{Z}_{22}] \end{bmatrix} \begin{pmatrix} \tilde{J}_z \\ \tilde{J}_x \end{pmatrix} \tag{21}$$

in which $[\tilde{Z}_{nm}]$ $(n, m = 1,2)$ are diagonal matrices if the transformed quantities $\tilde{E}_z$, $\tilde{E}_x$, $\tilde{J}_z$, and $\tilde{J}_x$ are written in vector notation.

Because the final boundary condition cannot be applied in the transformed domain, (21) has to be transformed back into the original domain [4]. For the example of Fig. 2, the metallic strip makes up the smaller part of the interface, so in this case the reverse transformation is performed only for the (reduced) number of lines that pass through the strip. The resulting equation

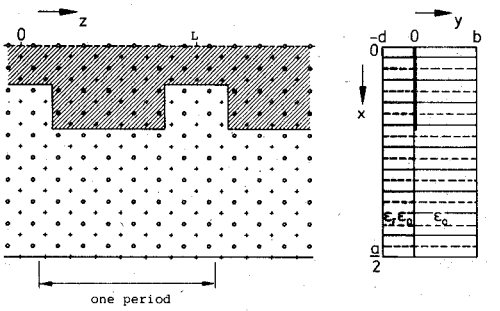

Fig. 3. Discretization lines for a periodic structure.

$$\begin{pmatrix} E_z \\ E_x \end{pmatrix}_{\text{red}} = \begin{bmatrix} [Z_{11}] & [Z_{12}] \\ [Z_{21}] & [Z_{22}] \end{bmatrix}_{\text{red}} \begin{pmatrix} J_z \\ J_x \end{pmatrix}_{\text{red}} = 0 \tag{22}$$

in which $[Z_{nm}]$ $(n, m = 1,2)$ are now full matrices, will have nontrivial solutions for the resonant frequencies of the structure only, which are found from the determinantal equation

$$\det[Z(f)]_{\text{red}} = 0. \tag{23}$$

At resonance, all field components can be derived from the current density distribution, which occurs as an eigenvector in (22).

III. Periodic Structures

The analysis of planar periodic structures proceeds similarly to the analysis of resonant structures described above.

For the periodic structure in Fig. 3, the potential functions and all electromagnetic field components must satisfy Floquet's theorem

$$\Psi^{e,h}(x, y, z + L) = e^{-j\beta L}\Psi^{e,h}(x, y, z) \tag{24}$$

where β is the propagation constant in the z-direction and L is the period length. For the x-direction homogeneous boundary conditions apply.

One period of the structure is discretized with Ψ^e lines located at $x = (i - 0.5)h_x$, $z = kh_z$, and Ψ^h lines at $x = ih_x$, $z = (k + 0.5)h_z$ $(i = 1, \cdots, N_x;\ k = 1, \cdots, N_z)$. The finite difference expression for the first derivative of Ψ^e with respect to z is then given by

$$h_z\frac{\partial\Psi^e}{\partial z} \rightarrow [\Psi^e][D_z]^t \tag{25}$$

with

$$[D_z] = \begin{bmatrix} -1 & 1 & & \\ & \ddots & \ddots & \\ & & & 1 \\ s & & & -1 \end{bmatrix}, \qquad s = e^{-j\beta L}. \tag{26}$$

The difference operator for Ψ^h and for $\partial\Psi^e/\partial z$ is $-[D_z]^{*t}$, which yields for the second-order derivative of Ψ^e

$$h_z^2\frac{\partial^2\Psi^e}{\partial z^2} \rightarrow -[\Psi^e][D_z]^t[D_z]^* = [\Psi^e][D_{zz}^e]^t. \quad (27)$$

The Hermitian matrix $[D_{zz}^e]$ is transformed into a diagonal matrix $[d_{zz}^e]$ by means of the unitary transformation matrix $[T_z^e]$

$$[T_z^e]^{*t}[D_{zz}^e][T_z^e] = \mathrm{diag}[d_{zz}^e] \quad (28)$$

where

$$[d_{zz}^e]_{kk} = -4\sin^2(\varphi_k/2) \quad (29)$$

and

$$[T_z^e]_{\iota k} = \sqrt{1/N}\, e^{j\iota\varphi k} \quad (30)$$

with

$$\varphi_k = \frac{2\pi(k-1)-\beta L}{N_z}. \quad (31)$$

On account of the periodic boundary conditions, one obtains a difference matrix $[D_{zz}^h]$ for Ψ^h equal to $[D_{zz}^e]$, so the same transformation matrix could be used. However, if the elements of $[T_z^h]$ are defined as

$$[T_z^h]_{\iota k} = \frac{j}{\sqrt{N}} e^{j(\iota+0.5)\varphi_k} \quad (32)$$

in which the shifting of lines is apparent, the expressions for the first derivatives in the transformed domain remain real, e.g.,

$$[T_z^h]^{*t}[D_z][T_z^e] = \mathrm{diag}[d_z] \quad (33)$$

with

$$[d_z]_{kk} = 2\sin(\varphi_k/2). \quad (34)$$

The continuity conditions for the tangential field components are again solved in the transformed domain. After the reverse transformation, the final boundary condition leads to a Hermitian matrix $[Z]_{\mathrm{red}}$, of which the determinant should vanish

$$\det[Z(\omega,\beta)]_{\mathrm{red}} = 0. \quad (35)$$

The solutions to this equation are typically represented as the dispersion curves in the $\omega-\beta$ diagram.

IV. Numerical Results

As a first example, a triangular microstrip resonator is considered. It should demonstrate that the analysis is not restricted to rectangular structures. The shielding dimensions are taken large enough to approximate unshielded structures. Fig. 4 shows that the resonant frequencies obtained with this method agree fairly well with the results from the transverse-resonance method and even better with the measurements, both from [5].

The accuracy of about 1 percent will be sufficient for most applications. If the resonant frequencies are used for calculating discontinuities, however, a much higher accuracy is required, as will be illustrated for the end effect of a shorted slotline.

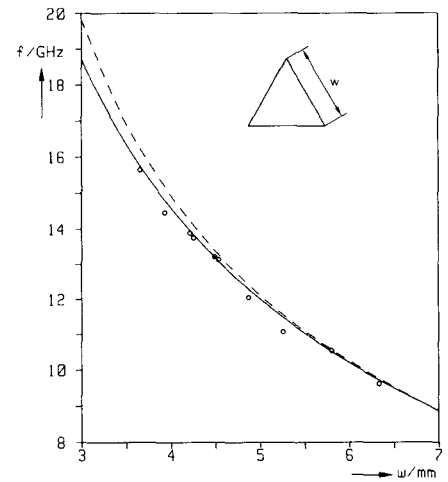

Fig. 4. Resonant frequency for a triangular microstrip resonator ($\epsilon_r = 9.7$, $d = 0.635$ mm, $b = 10d$). ——: this method, ---: transverse-resonance method [5], ∘ ∘ ∘ ∘: experiment [5].

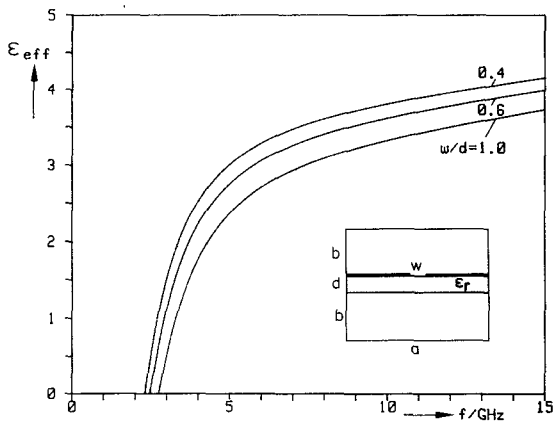

Fig. 5. Dispersion characteristics for shielded slotlines. ($\epsilon_r = 9.7$, $d = 0.635$ mm, $b = 10d$, $a = w + 20d$).

A slotline resonator with a cross-section and dispersion characteristic as depicted in Fig. 5 will have resonant frequencies given by

$$f = \frac{n}{2}\frac{c_0}{(L+2\Delta l)\sqrt{\epsilon_{\mathrm{eff}}}} \qquad (n = 1,2,\cdots) \quad (36)$$

where L is the resonator length.

The effective dielectric constant ϵ_{eff} is calculated by the method of lines from the cross-sectional problem with negligible error, so the resonant frequency has to be calculated with a relative error, which is about a factor $2\Delta l/L$ smaller than the error tolerated for the end effect Δl.

Fig. 6 shows the convergence behavior of the resonant frequencies in dependence on the discretization distance h_z. The position of the edges is fixed with respect to the discretization lines by means of the edge parameters p_x and p_z. This results in smooth convergence curves, so the discretization error may be represented in good approximation by a quadratic or cubic function, from which the extrapolated values for $h_z \rightarrow 0$ are easily derived. The final result is independent of the actual value of p_z.

In Fig. 6, the resonant frequency calculated with $p_z = 0.25$ and $h_z = 0.5$ mm has an error of about 1 percent. Taking

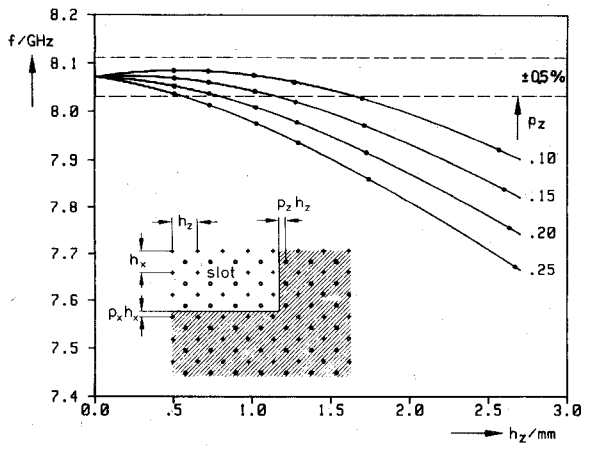

Fig. 6. Convergence behavior of the resonant frequency as a function of the discretization distance h_z and the edge parameter p_z. ($w = d$, $L = 20$ mm).

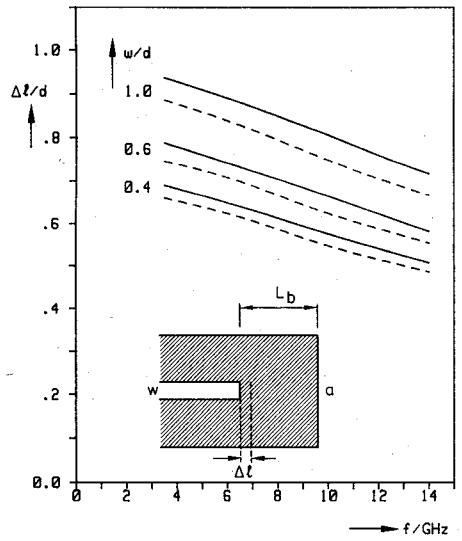

Fig. 7. End effect of a shorted slotline. (Dimensions as in Fig. 5; $L_b > 12$ mm, variable in order to avoid box resonances.) —— this method, ---- Jansen [6].

into account the results obtained at some larger discretization distances and applying a least squares method for quadratic or cubic extrapolation increases the accuracy by more than one order of magnitude. In this case, the error for the resonant frequency is estimated to be less than 0.1 percent, including the error from the discretization in the x-direction (about 0.02 percent with $p_x = 0.25$ and $h_x = 0.115$ mm). Thus, the end effect has an accuracy of about 2 percent.

In Fig. 7, the calculated end effect of a shorted slotline is shown as a function of frequency and compared with results from the literature [6]. For $\lambda/2$ resonators, the end effect was found to be a few percent larger, whereas resonators with one full wavelength or more gave identical results.

As a first example for the analysis of periodic structures a microstrip meander line is considered. Fig. 8 shows the calculated dispersion diagram. Up to about 9 GHz, this diagram may be approximated to some extent by considering the meander as a straight line and taking into account the propagation constants β_{even} and β_{odd} of the multiple coupled lines at $\beta L = 0, 2\pi, \cdots$, and $\beta L = \pi, 3\pi, \cdots$, respectively. The stopband, however, would not be obtained by such a simple method.

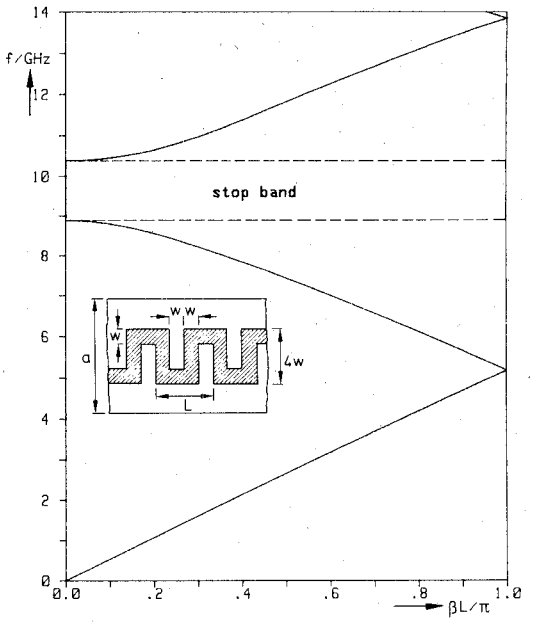

Fig. 8. Dispersion diagram of a microstrip meander line ($\epsilon_r = 2.3$, $w = 2.37$ mm, $d = 0.79$ mm, $b = 10d$, $a = 12w$, $L = 4w$).

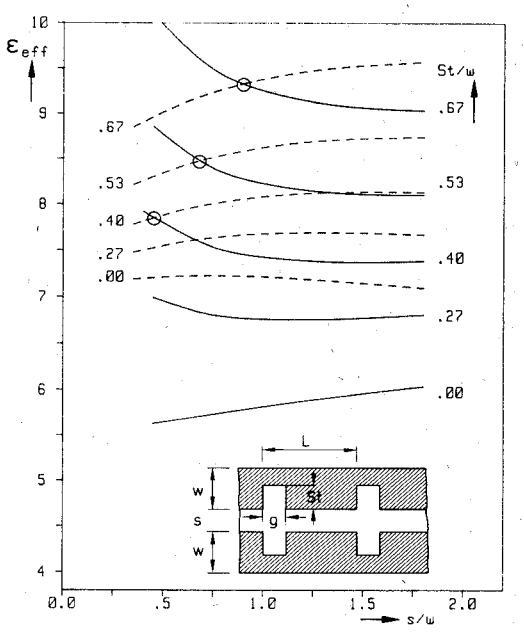

Fig. 9. Effect of periodic slotting on the phase velocities of coupled microstrip lines ($\epsilon_r = 9.6$, $f = 6$ GHz, $w = d = 0.635$ mm, $b = 10d$, $L = 4g = 0.15$ mm). —— odd mode, ---- even mode.

The final example demonstrates the use of periodic structures in coupled microstrip lines. The difference between the phase velocities of the even and odd mode of these lines leads to bad isolation in microstrip proximity couplers [3]. To eliminate this effect, transverse periodic slotting at the inner edges may be applied. Fig. 9 shows that the slotting has more influence on the odd mode than

TABLE I
FIRST-ORDER DIFFERENCE MATRICES IN THE ORIGINAL AND THE TRANSFORMED DOMAIN FOR THE VARIOUS (N FOR NEUMANN, D FOR DIRICHLET) BOUNDARY CONDITIONS FOR Ψ^e

boundary conditions left - right	[D]	[d]	elements of [d] ≠ 0
N - D	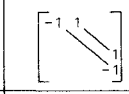		$[d]_{i,i} = -2 \sin \frac{(i-.5)\pi}{2N+1}$ $(i=1,\ldots,N)$
D - N	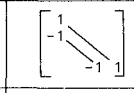		$[d]_{i,i} = 2 \sin \frac{(i-.5)\pi}{2N+1}$ $(i=1,\ldots,N)$
D - D	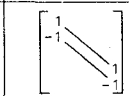		$[d]_{i+1,i} = 2 \sin \frac{i\pi}{2N+2}$ $(i=1,\ldots,N)$
N - N	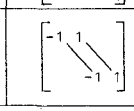		$[d]_{i-1,i} = -2 \sin \frac{(i-1)\pi}{2N}$ $(i=2,\ldots,N)$

TABLE II
ELEMENTS OF THE TRANSFORMATION MATRICES

boundary conditions left - right	$[T^e]_{ik}$	$[T^h]_{ik}$
N - D	$\sqrt{\frac{2}{N+.5}} \cos \frac{(i-.5)(k-.5)\pi}{N+.5}$ $(i,k=1,\ldots,N)$	$\sqrt{\frac{2}{N+.5}} \sin \frac{i(k-.5)\pi}{N+.5}$ $(i,k=1,\ldots,N)$
D - N	$\sqrt{\frac{2}{N+.5}} \sin \frac{i(k-.5)\pi}{N+.5}$ $(i,k=1,\ldots,N)$	$\sqrt{\frac{2}{N+.5}} \cos \frac{(i-.5)(k-.5)\pi}{N+.5}$ $(i,k=1,\ldots,N)$
D - D	$\sqrt{\frac{2}{N+1}} \sin \frac{ik\pi}{N+1}$ $(i,k=1,\ldots,N)$	$\sqrt{\frac{2}{N+1}} \cos \frac{(i+.5)k\pi}{N+1}$; $k>0$ $\sqrt{\frac{1}{N+1}}$; $k=0$ $(i,k=0,1,\ldots,N)$
N - N	$\sqrt{\frac{2}{N}} \cos \frac{(i-.5)(k-1)\pi}{N}$; $k>1$ $\sqrt{\frac{1}{N}}$; $k=1$ $(i,k=1,\ldots,N)$	$\sqrt{\frac{2}{N}} \sin \frac{(i-1)(k-1)\pi}{N}$ $(i,k=2,\ldots,N)$

on the even mode, so it is possible to achieve a phase-equalization.

APPENDIX

Because the discretizations in both directions may be treated fully independently, the difference and transformation matrices are summarized for one-dimensional discretization only. The difference matrices depend on the lateral boundary conditions. In Fig. 2, for example, the Neumann condition ($\partial\Psi^e/\partial x = 0$) at $x = 0$ and the Dirichlet condition ($\Psi^e = 0$) at $x = a/2$ are taken into account by putting $\Psi^e_{0,k} = \Psi^e_{1,k}$ and $\Psi^e_{N_x+1,k} = 0$ in (3).

The difference and transformation matrices for the various combinations of the lateral boundary conditions of Ψ^e are shown in Tables I and II. The number of lines for Ψ^e is denoted by N, which should be replaced by N_x and N_z for the respective directions.

If one of the potential functions Ψ^e and Ψ^h has Neumann conditions on both side walls, it will have one discretization line and one spectral component (a dc component) more than the other one, which results in rectangular matrices $[D]$ and $[d]$.

The transformations are all derived from the elementary relation $[D][T^e] = [T^h][d]$, e.g.,

$$\begin{aligned}[T^e_x]^t[D^e_{xx}][T^e] &= -[T^e_x]^t[D_x]^t[T^h_x][T^h_x]^t[D_x][T^e_x] \\ &= -[d_x]^t[d_x] \\ &= \operatorname{diag}[d^e_{xx}].\end{aligned}$$

REFERENCES

[1] U. Schulz and R. Pregla, "A new technique for the analysis of the dispersion characteristics of planar waveguides," *Arch. Elec. Übertragung.*, vol. 34, pp. 169–173, 1980.

[2] U. Schulz and R. Pregla, "A new technique for the analysis of planar waveguides and its application to microstrips with tuning septums," *Radio Sci.*, vol. 16, pp. 1173–1178, 1981.

[3] F. C. de Ronde, "Wide-band high directivity in MIC proximity couplers by planar means," in *Proc. MTT Int. Symp.*, (Washington, D.C.), 1980.

[4] S. B. Worm, "Analysis of planar microwave structures with arbitrary contour (in German)," Ph.D. Thesis, Fernuniversitaet Hagen, 1983.

[5] W. T. Nisbet and J. Helszajn, "Mode charts for microstrip resonators on dielectric and magnetic substrates using a transverse-resonance method," *Microwaves Opt. Acoust.*, vol. 3, pp. 69–77, 1979.

[6] R. H. Jansen, "Hybrid mode analysis of end effects of planar microwave and millimeterwave transmission lines," *Inst. Elec. Eng. Proc.*, part H, vol. 128, pp. 77–86, 1981.

Stephan B. Worm was born in Bladel, the Netherlands, in 1951. He received the M.Sc. degree from the Eindhoven University of Technology, Eindhoven, the Netherlands, in 1978, and the Ph.D. degree from the Fernuniversitaet in Hagen, Germany, in 1983.

From 1978 to 1983, he was employed at the Fernuniversitaet, Hagen, where he was engaged in theoretical investigations of the properties of planar microwave structures. In 1983, he joined Philips, Elcoma Division, where he is engaged in the development of microwave tubes.

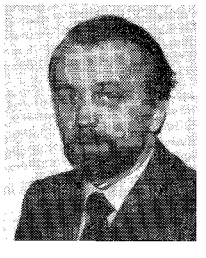

Reinhold Pregla (M'76) was born in Luisenthal, on August 5, 1938. He received the master's degree in electrical engineering (Dipl.-Ing.) and his doctorate of engineering (Dr.-Ing.) from the Technische Universität Braunschweig, West Germany, in 1963 and 1966, respectively.

From 1966 to 1969, he was a Research Assistant at the Department of Electrical Engineering of the Technische Universität Braunschweig (Institut für Hochfrequenztechnik), where he was engaged in investigations on microwave filters. After the Habilitation, he was a Lecturer in high frequencies at the Technische Universität, Bochum, West Germany. Since 1975, he has held a position as full Professor in electrical engineering at the Fernuniversität (a university for distance study) in Hagen, West Germany. His fields of investigations are microwave filters, waveguide theory, and antennas.